

A MUSTA-FORCE algorithm for solving partial differential equations of relativistic hydrodynamics

J. Porter-Sobieraj¹, M. Słodkowski², D. Kikoła², J. Sikorski³
P. Aszklar¹

¹ Warsaw University of Technology, Faculty of Mathematics and Information Science, Koszykowa 75, 00-662 Warsaw, Poland

² Warsaw University of Technology, Faculty of Physics, Koszykowa 75, 00-662 Warsaw, Poland

³ University of Warsaw, Faculty of Physics, Hoża 69, 00-681 Warsaw, Poland,

Abstract

Understanding event-by-event correlations and fluctuations is crucial for the comprehension of the dynamics of heavy ion collisions. Relativistic hydrodynamics is an elegant tool for modeling these phenomena; however, such simulations are time-consuming, and conventional CPU calculations are not suitable for event-by-event calculations. This work presents a feasibility study of a new hydrodynamic code that employs graphics processing units together with a general MUSTA-FORCE algorithm (Multi-Stage Riemann Algorithm - First Order Centered scheme) to deliver a high-performance yet universal tool for event-by-event hydrodynamic simulations. We also investigate the performance of selected slope limiters that reduce the amount of numeric oscillations and diffusion in the presence of strong discontinuities and shock waves. The numerical results are compared to the exact solutions to assess the code's accuracy.

Keywords: relativistic hydrodynamic, simulation of heavy ion collisions, quark-gluon plasma, high energy nuclear physics, numerical algorithms, MUSTA-FORCE, parallel computing, CUDA/GPU

1 Motivation

Relativistic hydrodynamics simulations are widely used in the modeling of nuclear processes in high-energy nuclear physics when examining the properties of the quark gluon plasma (QGP). Detailed information regarding the reactions that take place at the microscopic level is not required. Hydrodynamic model formalism treats QGP as a perfect fluid and assumes a single equation of state. The bulk and hot nuclear system can be described using hydrodynamic conservation laws and then solved numerically [1, 2]. Hydrodynamic models are extremely successful in describing experimental results for particles with low transverse momentum which is a behavior of bulk nuclear matter. On the other hand, jets (narrow spays of hadrons and other particles produced by the hadronization of a high energy quark or gluon) are widely used to probe the properties of the QGP. This is an approach analogous to tomography: an external, penetrating probe, whose properties (like a production mechanism) are under experimental and theoretical control, is shot through the medium. We can then infer the properties of the analyzed system from the modification of the probe's energy. Jets are such probes - external to the QGP. Because their production requires a large momentum transfer, they are produced very early in the collision, in the initial hard interaction, before the QGP phase. Their production is described well by perturbative quantum chromodynamics (pQCD) calculations. Thus they are excellent tools for QGP research.

The mechanism involved in energy loss due to interactions with nuclear matter has been a topic of extensive theoretical and experimental studies over the last two decades. However, the energy dissipated by jets can also alter the properties of bulk nuclear matter (for instance, so-called elliptic flow) in the intermediate transverse momentum range. There is little understanding of such effects. For such studies, we need to efficiently model the soft particle evolution with a high spatial resolution to capture the jet-induced modification of the characteristics of the bulk nuclear matter. Moreover, the Cartesian coordinate system is preferred to ensure a high spatial resolution that is constant throughout the evolution of the system. Such calculations are necessary to fully understand the proprieties of this unique state of nuclear matter.

The main motivation of our work is therefore to develop a new application to study the physics of heavy ion collisions, enabling the execution of hydrodynamic simulations on high-resolution Cartesian grids. The goal is to combine two areas of heavy ion physics that are usually treated separately: bulk physics, described by hydrodynamic models, and the physics of jets. Such an approach will allow us to investigate in detail how energy deposited by jets affects the behavior of soft particles. In turn, it will help to understand

better the properties of nuclear matter under extreme conditions.

Moreover, event-by-event correlations and fluctuations play a significant role in the understanding of heavy ion collision dynamics. Unfortunately, hydrodynamic simulations are time- and computing-power-consuming, and event-by-event calculations are challenging when conventional CPU computing is used. The achievements of hydrodynamic models in high-energy physics motivated us to work on a new high-performance program that facilitates event-by-event simulation with high numerical precision using graphics processing units.

Equations of ideal relativistic hydrodynamics in one spatial dimension can be solved both analytically and numerically as shown e.g. in [3, 4, 5]. On a three dimensional grid, however, an analytical solution is difficult to achieve and the problem needs to be addressed via numerical algorithms. A number of such algorithms already exist solving relativistic hydrodynamic equations for ideal and viscous fluid models either directly [6, 7, 8, 9, 10] or retrieving the solution from a particle-based kinematic model [11]. These solutions, however, incur a heavy computational cost in 3+1 dimensions. Hence, to ensure reasonable performance, the simulation is often done in reduced dimensionality, or one of the dimensions (usually rapidity) is represented in low resolution, by only a few layers. This approach is motivated by certain symmetries that are approximately held in heavy ion collisions. Full (3+1)-dimensional, high resolution simulations are currently very time-consuming computations for traditional, single-threaded software.

This problem can be solved by employing general purpose computing on graphics processing units (GPGPU). The paper [12] has shown that a GPGPU-based implementation of the SHASTA algorithm [13] can provide up to two orders of magnitude improvement in performance. In addition, our previous work, based on the universal multi-stage (MUSTA-FORCE) algorithm [14, 15] also proved that hydrodynamic computations can be performed within a reasonable timeframe. Although the implemented method has a high numerical cost and complexity, it scales perfectly with parallel computations. Our implementation turned out to be over 200 times faster than a sequential implementation on a CPU [16]. It produces good statistics and high spacial and temporal resolutions at the same time.

The speed-up gained by using a GPU made it possible to develop a valuable new tool for high energy nuclear science. Our current GPU implementation allows a device to perform a massive number of simulations, and furthermore, the MUSTA-FORCE algorithm is a very universal tool. Its strength lies in the fact that it uses simple central schemes and does not require any knowledge of the physical process's details. However, in the case of large gradients it is necessary to apply a slope limiter to reduce numerical oscillations. Therefore,

we focused here on how to improve the accuracy of the MUSTA-FORCE algorithm. The hydrodynamic simulation results presented in this paper show that the MUSTA-FORCE method is very sensitive to the choice of slope and slope limiter, and the way that it is applied. We used such a procedure for each dimension separately, but in general it could be applied in other ways (e.g. a common slope limiting value could be chosen for all the variables). There is no general procedure in a multi-dimensional and non-scalar case, and always some experimentation is necessary for both a particular system of equations, and perhaps even a particular problem. Under the conditions of our simulation the schemes must be especially sensitive to problems containing both strong discontinuities and smooth solution features.

The paper is organized as follows. The MUSTA-FORCE algorithm, together with the slope limiters, is described in detail in Section 2. Section 3 presents the results of using such slope limiters for standard benchmarks in nuclear physics and compares them with known analytical solutions. We discuss their ability to achieve high order accuracy in smooth regions while maintaining stable, non-oscillatory and sharp discontinuity transitions. The last section concludes our paper.

2 Hydrodynamics Simulations

2.1 Mathematical Description

Relativistic hydrodynamics simulations are based on hyperbolic partial differential equations in the form:

$$\frac{\partial U}{\partial t} + \frac{\partial F(U)}{\partial x} + \frac{\partial G(U)}{\partial y} + \frac{\partial H(U)}{\partial z} = 0 \quad (1)$$

and an equation of state:

$$p = p(e, n) \quad (2)$$

$U = (E, M_x, M_y, M_z, R)$ is a vector of conserved quantities in the *laboratory rest frame*; E is the energy density, M_x , M_y and M_z are the momentum densities in the x , y and z Cartesian coordinates, respectively, and R is a conserved charge density. Vectors of fluxes F , G , H in the x , y , and z

directions are defined as:

$$\begin{aligned}
F(U) &= \begin{bmatrix} (E+p)v_x \\ M_x v_x + p \\ M_y v_x \\ M_z v_x \\ Rv_x \end{bmatrix} \\
G(U) &= \begin{bmatrix} (E+p)v_y \\ M_x v_y \\ M_y v_y + p \\ M_z v_y \\ Rv_y \end{bmatrix} \\
H(U) &= \begin{bmatrix} (E+p)v_z \\ M_x v_z \\ M_y v_z \\ M_z v_z + p \\ Rv_z \end{bmatrix}
\end{aligned} \tag{3}$$

where v is the velocity, and p is pressure, defined by the energy e and charge density n in the *fluid rest frame*, where velocity v vanishes ($v = (0, 0, 0)$). Additionally, the following relations occur:

$$\begin{aligned}
E &= (\varepsilon + p)\gamma^2 - p \\
M_i &= (\varepsilon + p)\gamma^2 v_i, \quad i = x, y, z \\
R &= n\gamma
\end{aligned} \tag{4}$$

where ε is the energy density and $\gamma = \frac{1}{\sqrt{1-v^2}}$ is the Lorentz factor. Eq. 4 defines the transformation from *rest frame* variables to *conserved* variables used in integration.

2.2 Initial Conditions

To start hydrodynamic evolution, an initial state is required as input.

The most basic is parametrizations based e.g. on Glauber-like models in the transverse plane (see [17] for a review), and Bjorken's solution in the longitudinal direction.

Other approaches involve models based on color glass condensate (CGC), which describe a Lorentz contracted and slowed down, fast moving particle; pQCD+saturation model [18], or the string rope model [19].

These models describe a smooth, averaged initial state. However, since the hydrodynamic equations are nonlinear, a solution with an averaged initial state is not equivalent to the average of solutions with fluctuating initial conditions. Because of this, event-by-event calculations became a major point of interest.

Fluctuating initial conditions can be obtained using e.g. Monte–Carlo Glauber [20, 21, 22] or CGC, SPheRIO, NeXus [23], NeXSPhRIO [24], and models like EPOS [25] or UrQMD [26].

2.3 Time Integration

For time propagation the standard Runge–Kutta methods are employed [29]. For numerical stability only total variation diminishing methods are used.

In general, a Runge–Kutta method for Eq. 1 can be written in the form:

$$\begin{aligned}
 U_{(0)}^n &= U^n \\
 U_{(i)}^n &= \sum_{k=0}^{i-1} (\alpha_{ik} U_{(k)}^n + \Delta t \beta_{ik} L(U_{(k)}^n)), \\
 & \quad i = 1, \dots, m \\
 U^{n+1} &= U_{(m)}^n
 \end{aligned} \tag{5}$$

where the upper index without parentheses denotes the time step, the lower index denotes integration step, L is a numerical recipe to calculate the negative flux gradient in Eq. 1 and α, β are constant coefficients given for a particular method.

For second order accuracy the following method is used:

$$\begin{aligned}
 U_{(1)}^n &= U^n + \Delta t L(U^n) \\
 U^{n+1} &= \frac{1}{2} (U^n + U_{(1)}^n + \Delta t L(U_{(1)}^n))
 \end{aligned} \tag{6}$$

and for third order accuracy:

$$\begin{aligned}
 U_{(1)}^n &= U^n + \Delta t L(U^n) \\
 U_{(2)}^n &= \frac{3}{4} U^n + \frac{1}{4} U_{(1)}^n + \frac{1}{4} \Delta t L(U_{(1)}^n) \\
 U^{n+1} &= \frac{1}{3} U^n + \frac{2}{3} U_{(2)}^n + \frac{2}{3} \Delta t L(U_{(2)}^n)
 \end{aligned} \tag{7}$$

It is apparent that apart from the additional computational cost due to more evaluations of L , these methods introduce the need for an additional storage register for each of the conserved variables. As this can be an issue for large resolution simulations, a low storage version of the third order method can be used.

2.4 Hybrid MUSTA-FORCE Algorithm

To obtain a general and accurate solution for Eq. 1 and Eq. 2, we use a hybrid Multi-STAge (MUSTA) approach [15, 27]. This utilizes a centered flux in a predictor–corrector loop, solving the Riemann problem numerically, i.e. without using a priori information about waves.

In order to calculate flux $F_{i+\frac{1}{2}}$ the algorithm, in a one dimensional case, is as follows:

1. Introduce auxiliary variables $U_L^{(l)}$ and $U_R^{(l)}$ and their fluxes $F_L^{(l)}$ and $F_R^{(l)}$.
2. Set $U_L^0 = U_i$, $U_R^0 = U_{i+1}$.
3. Calculate $F_{i+\frac{1}{2}}^{(l)}$ using a centered flux, $U_L^{(l)}$, $U_R^{(l)}$, $F_L^{(l)}$ and $F_R^{(l)}$. If l reached a maximum number of iterations, stop.
4. Solve Riemann problem locally:

$$\begin{aligned} U_L^{(l+1)} &= U_L^{(l)} - \frac{\Delta t}{\Delta x} \left(F_{i+\frac{1}{2}}^{(l)} - F_L^{(l)} \right), \\ U_R^{(l+1)} &= U_R^{(l)} - \frac{\Delta t}{\Delta x} \left(F_R^{(l)} - F_{i+\frac{1}{2}}^{(l)} \right). \end{aligned} \quad (8)$$

5. Go back to step 3.

As a centered flux in step 3, we use the First ORder CEntered (FORCE) scheme:

$$F_{i+\frac{1}{2}}^{\text{force}} = \frac{1}{2} \left(F_{i+\frac{1}{2}}^{\text{lw}} + F_{i+\frac{1}{2}}^{\text{lf}} \right) \quad (9)$$

where $F_{i+\frac{1}{2}}^{\text{lw}}$ is the Lax-Wendroff type flux:

$$F_{i+\frac{1}{2}}^{\text{lw}} = F \left(\frac{1}{2}(U_L + U_R) - \frac{\alpha \Delta t}{2\Delta x}(U_R - U_L) \right) \quad (10)$$

and $F_{i+\frac{1}{2}}^{\text{lf}}$ is the Lax-Friedrichs type flux:

$$F_{i+\frac{1}{2}}^{\text{lf}} = \frac{1}{2}(F_L + F_R) - \frac{\Delta x}{2\alpha \Delta t}(U_R - U_L) \quad (11)$$

In a three-dimensional case $\alpha = 3$, but other values may also be considered.

To achieve second order accuracy in space and time, we extend our algorithm with the MUSCL-Hancock scheme. The basic idea of this scheme is to use more cells to interpolate inter-cell values and evolve them half a time step:

1. Replace cell average values U_i^n by a piecewise linear function inside i -th cell:

$$U_i(x) = U_i^n + \frac{(x - x_i)}{\Delta x} \Delta_i \quad (12)$$

where Δ_i is a slope vector and will be defined later.

In the local coordinates the points $x = 0$ and $x = \Delta x$ correspond to boundaries of the cell $x_{i-\frac{1}{2}}$ and $x_{i+\frac{1}{2}}$. The values at these points are $U_i^L = U_i^n - \Delta_i/2$ and $U_i^R = U_i^n + \Delta_i/2$.

2. Propagate U_i^L and U_i^R by a time $\frac{1}{2}\Delta t$:

$$\begin{aligned} \tilde{U}_i^L &= U_i^L + \frac{1}{2} \frac{\Delta t}{\Delta x} (F(U_i^L) - F(U_i^R)) \\ &\quad + \frac{1}{2} \frac{\Delta t}{\Delta y} (G(U_i^L) - G(U_i^R)) \\ &\quad + \frac{1}{2} \frac{\Delta t}{\Delta z} (H(U_i^L) - H(U_i^R)) \\ \tilde{U}_i^R &= U_i^R + \frac{1}{2} \frac{\Delta t}{\Delta x} (F(U_i^L) - F(U_i^R)) \\ &\quad + \frac{1}{2} \frac{\Delta t}{\Delta y} (G(U_i^L) - G(U_i^R)) \\ &\quad + \frac{1}{2} \frac{\Delta t}{\Delta z} (H(U_i^L) - H(U_i^R)) \end{aligned} \quad (13)$$

3. Use \tilde{U}_i^L and \tilde{U}_i^R as U_L^0 and U_R^0 in MUSTA.

A simple choice for the *slope* Δ_i in Eq. 12 is:

$$\Delta_i = \frac{1}{2}(U_{i+1}^n - U_{i-1}^n) \quad (14)$$

which indeed results in a second-order accurate algorithm. However, as predicted by Godunov's theorem, it has the unpleasant effect of producing spurious oscillations in the case of strong gradients. Complex study of MUSTA schemes can be found in [28].

2.5 Slope Limiters in the MUSTA-FORCE

To avoid such oscillations and to solve problems that appear in the presence of shocks, discontinuities or sharp changes, flux limiting and slope limiting

methods have been proposed [30, 31]. We employed a slope limiting method; instead of Δ_i as in Eq. 14 we use

$$\tilde{\Delta}_i = \xi(r_i)(U_i - U_{i-1}) \quad (15)$$

in Eq. 12, where ξ is called the slope limiter and

$$r_i = \frac{U_{i+1} - U_i}{U_i - U_{i-1}}. \quad (16)$$

Then one can calculate U_i^L and U_i^R using the following relations

$$\begin{aligned} U_i^L &= U_i - \frac{1}{2}\xi(1/r_i)(U_{i+1} - U_i), \\ U_i^R &= U_i + \frac{1}{2}\xi(r_i)(U_i - U_{i-1}). \end{aligned} \quad (17)$$

There are a number of possible choices for ξ , each with its own characteristics and features. The four different limiters investigated in this paper are Minbee (MB) [32], Superbee (SB) [33], van Albada (VA) [34] and van Leer (VL) [35]. They are expressed as:

$$\xi_{\text{MB}}(r) = \max(0, \min(1, r)) \quad (18)$$

$$\xi_{\text{SB}}(r) = \max(0, \min(2r, 1), \min(r, 2)) \quad (19)$$

$$\xi_{\text{VA}}(r) = \frac{r^2 + r}{r^2 + 1} \quad (20)$$

$$\xi_{\text{VL}}(r) = \frac{r + |r|}{1 + |r|} \quad (21)$$

All the four limiters are symmetric, i.e. they meet the symmetry property:

$$\xi\left(\frac{1}{r}\right) = \frac{\xi(r)}{r} \quad (22)$$

that provides that forward and backward gradients are treated in the same manner. Otherwise, the results on the left would differ from those on the right despite initial symmetry in the system.

The limiters are designed to reduce the scheme to first order accuracy near shocks, and keep higher order in smooth areas. Introducing non-linearity in this way reduces spurious oscillations and retains good accuracy of the solution.

The two most extreme slope limiters are Minbee and Superbee. The first one is the most dissipative and the second - the least. Between them lies the admissible region for second order total variation diminishing (TVD) limiters.

Here it should also be stressed, that results are very sensitive to the choice of slope in Eq. 14 and the slope limiter—both the formula for ξ , and the way that it is applied.

2.6 Calculating the hydrodynamic flux

To complete the chapter about numerical methods for relativistic hydrodynamics, one more detail must still be dealt with. It is easy to change from rest frame variables and velocities to the conserved variables used in the integration. The inverse transformation, however, is not trivial.

It is needed, however, each time we compute the flux, since the equation of state (2) is defined as a function of e and n , and not E and R . As in [36], we can invert equations (4) and get

$$\begin{aligned}
 e &= E - Mv \\
 n &= R\sqrt{1 - v^2} \\
 v &= \frac{M}{E + p(e, n)} \\
 &= \frac{M}{E + p(E - Mv, R\sqrt{1 - v^2})}
 \end{aligned}
 \tag{23}$$

The set of equations (23) can be solved numerically, starting from the last one as the fixed point equation for v .

3 Discussion and Results

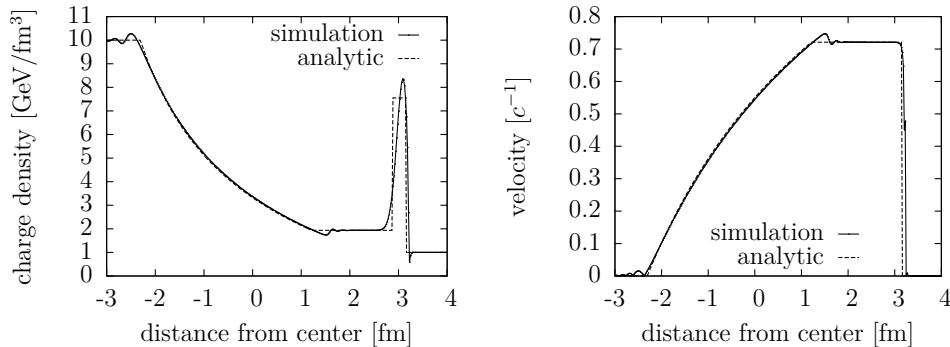


Figure 1: Sod shock tube, charge density in the local rest frame of the fluid (left) and velocity (right), MUSTA-FORCE with no limiter.

3.1 Implementation Notes

In the case of hydrodynamics simulations, fully (3+1)-dimensional simulations in space and in time are much-desired, to describe the system's evolution

without any assumptions regarding its symmetries and without decreasing the dimension of the problem. Moreover, event-by-event calculations become a major point of interest, with fluctuating initial conditions and with a large amount of statistics. Such simulations are extremely expensive in terms of computing power and require an efficient and fast computer code.

Therefore, we implemented the hydrodynamics simulation algorithm on a GPU using an NVIDIA CUDA framework [37]. Due to the large numerical grids in the simulations and the complexity of the computations, we used surface memory to store the simulation data. The state of the system is saved as 5 single precision floating-point numbers per lattice cell – the energy density, conserved charge density, and 3 momenta density; all in the *laboratory reference frame*. The maximum grid that fits then within the surface memory limitations is 240^3 .

3.2 Numerical Experiments

To verify the simulation reliability, the MUSTA-FORCE algorithm itself was tested (along with the four slope limiters – Minbee, Superbee, van Albada and van Leer) against three analytical solutions to relativistic hydrodynamics – the Sod shock tube [38, 39], the Hubble-like expansion [40] and ellipsoidal flow [41, 42]. For each of them, plots of chosen variables are presented together with the theoretical curves.

The number of stages and the order of Runge–Kutta method were fitted experimentally. In all the presented cases four MUSTA stages guaranteed stability and good numerical accuracy in acceptable calculation time on GPU. The third order accurate Runge–Kutta method was used for time integration.

Many numerical experiments for different parameters were carried out

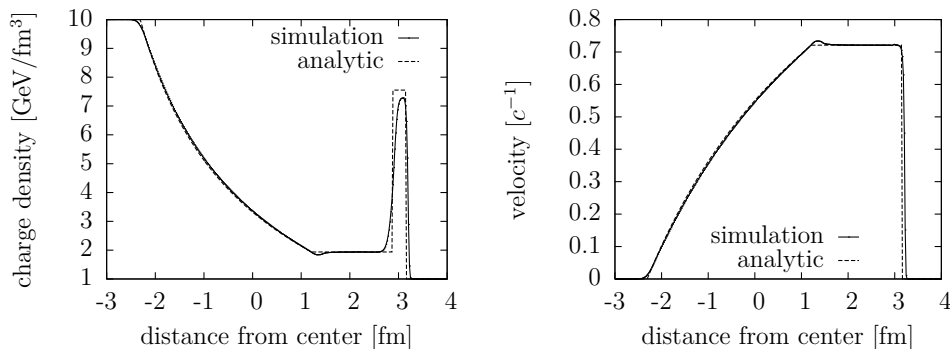


Figure 2: Sod shock tube, charge density in the local rest frame of the fluid (left) and velocity (right), MUSTA-FORCE with with Minbee limiter.

to verify correctness, convergence and robustness of the MUSTA-FORCE method. We present here the results for one representative set of parameters per analytical solution. The initial conditions and parameters like time step Δt and grid spacing Δx , Δy and Δz were given for each experiment separately. In all the cases the Courant number was less than 1. More detailed analysis of CFL numbers and stability limits in the MUSTA approach can be found in [43].

3.2.1 Sod Shock Tube

The first test is a solution to the Riemann problem. This is a one dimensional solution, whose initial state comprises two regions of stationary fluid with a charge and pressure discontinuity in the middle.

When the discontinuity is big enough, a relativistic shock wave appears in the solution. The initial conditions (given in Table 1 together with other parameters) were chosen to produce such a shock wave.

parameter	value
grid size	500
grid spacing	0.02
time step	0.005
p_L	$13\frac{1}{3}$
p_R	0
n_L	10
n_R	1

Table 1: Parameters of the Sod shock tube simulations

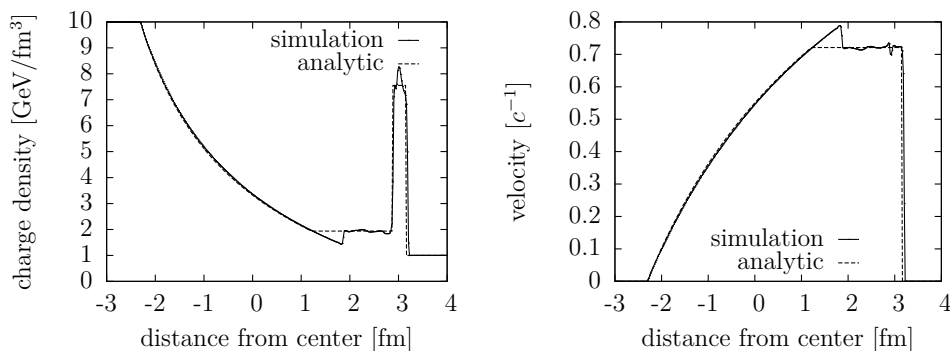


Figure 3: Sod shock tube, charge density in the local rest frame of the fluid (left) and velocity (right), MUSTA-FORCE with Superbee limiter.

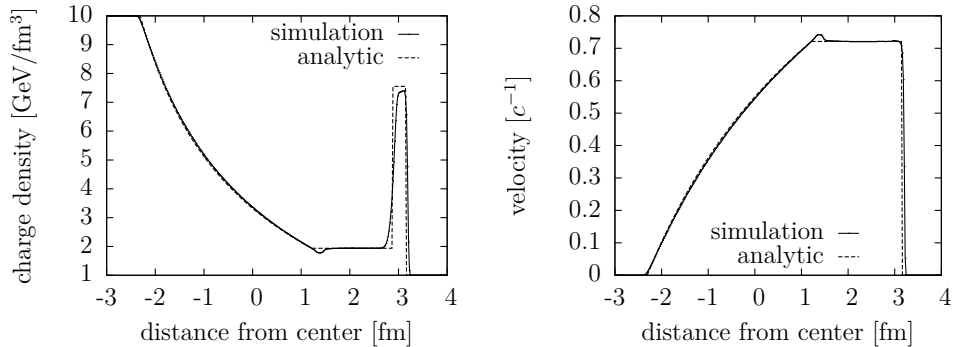


Figure 4: Sod shock tube, charge density in the local rest frame of the fluid (left) and velocity (right), MUSTA-FORCE with van Albada limiter.

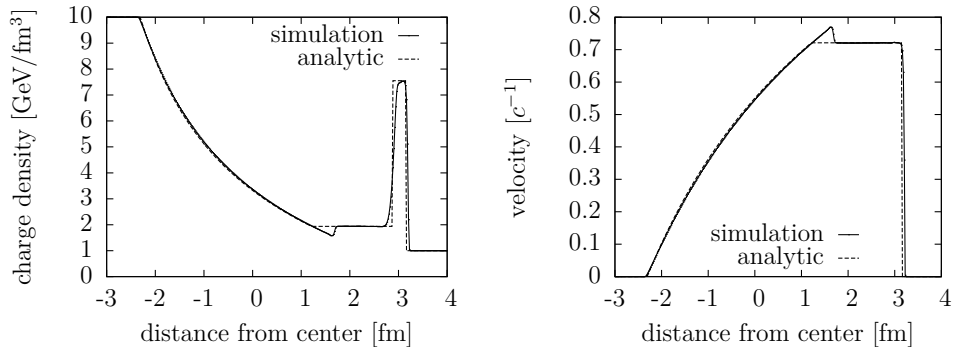


Figure 5: Sod shock tube, charge density in the local rest frame of the fluid (left) and velocity (right), MUSTA-FORCE with van Leer limiter.

The solution is divided into waves: the shock wave, the contact discontinuity, and the rarefaction wave.

The results are presented in Figs. 1–5.

For the *no limiter* case (Fig. 1) with the MUSTA-FORCE algorithm, oscillations at the contact points of waves become visible. The shock is also smeared out from the left side. For Minbee (Fig. 2) the overshoot is almost entirely gone, at the cost of some visible diffusion, especially in the shock wave region. Superbee in Fig. 3 is the most compressive limiter. The shocks are sharpened, but additional oscillations are introduced. Also the overshoot clearly visible in the velocity plot is enhanced. The van Albada limiter in Fig. 4 trades some sharpness for better rendition of the velocity profile; and for van Leer (Fig. 5) the shocks are sharp and the oscillations are gone, but the overshoot is still significant.

To sum up, van Albada and the Minbee limiter seem to be closest to the

analytic solution, and those two will be presented in rest of the tests.

3.2.2 Hubble-like Expansion

This is a three-dimensional, spherically symmetrical solution of matter that expands uniformly. The velocity is proportional to the distance from the center $v = \frac{\vec{r}}{t}$. The energy density is given by:

$$e = e_0 \left(\frac{\tau_0}{\sqrt{t^2 - r^2}} \right)^{3(1+c_s^2)} \quad (24)$$

In our case the solution is well defined for $r < t$. For the test we set $r < t - 0.5$ fm and put a vacuum ($e = v = 0$) outside this region. This means that the solution is exact only in the central area—on the periphery the matter will expand into the vacuum, so a rarefaction wave is expected. The solution uses an ultra-relativistic equation of state $p = c_s^2 e$.

Initial parameters are given in Table 2.

parameter	value
grid size	120^3
grid spacing	0.1
time step	0.03
e_0	1
c_s^2	$\frac{1}{3}$
τ_0	4
t_0	2

Table 2: Parameters of the Hubble-like expansion simulations

The results are presented in Fig. 6 and Fig. 7. $y = z = 0$ sections are shown through the three dimensional solution.

The results are similar to those in the previous test. The schemes were accurate in the middle region, and the Minbee limiter has shown less diffusion than van Albada at the sides.

3.2.3 Ellipsoidal Flow

The last test uses the ellipsoidal solution, which is a generalized Hubble-like solution (with velocity proportional to \vec{r}), a gaussian profile and vanishing pressure $p = 0$. The variables are given by the following equations:

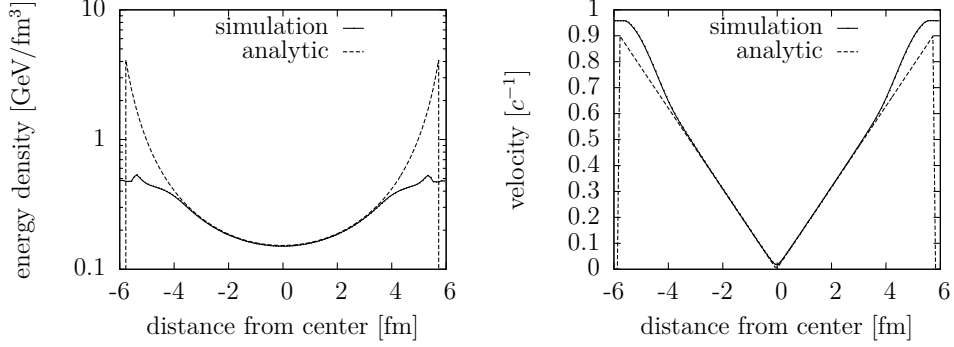


Figure 6: Hubble-like expansion, energy density in the local rest frame of the fluid (left) and velocity (right), MUSTA-FORCE with Minbee limiter.

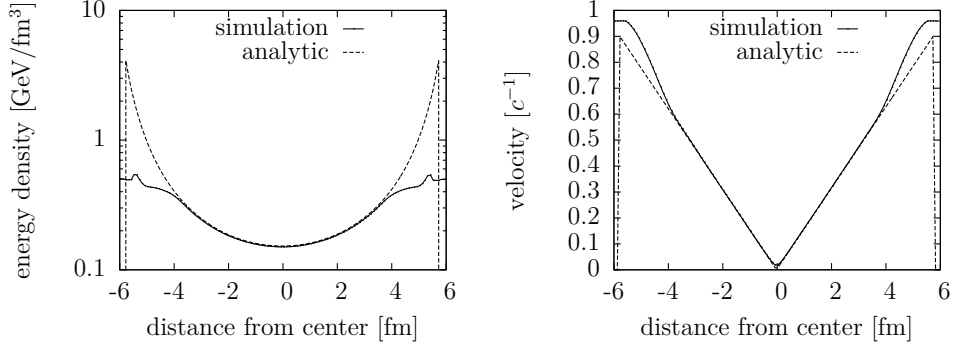


Figure 7: Hubble-like expansion, energy density in the local rest frame of the fluid (left) and velocity (right), MUSTA-FORCE with van Albada limiter.

$$e = \frac{C_e}{\prod_i (t + T_i)} \exp\left(-b_e^2 \frac{t^2}{\tau^2}\right) \quad (25)$$

$$n = \frac{C_n}{\prod_i (t + T_i)} \exp\left(-b_n^2 \frac{t^2}{\tau^2}\right) \quad (26)$$

$$\vec{v} = \left(\frac{a_1(t)x}{t}, \frac{a_3(t)y}{t}, \frac{a_2(t)z}{t}\right) \quad (27)$$

where $\tau = \sqrt{t^2 - \sum_i a_i^2 x_i^2}$, $a_i \equiv a_i(t) = t/(t + T_i)$ and C_e , C_n , b_e , b_n , T_i are constants; $i = 1, 2, 3$.

Initial parameters are given in Table 3.

The results are presented in Fig. 8 and Fig. 9. $y = z = 0$ sections are

parameter	value
grid size	120^3
grid spacing	0.1
time step	0.02
t_0	2
C_e	2
C_n	0.75
b_e	1
b_n	1
T_1	0.4
T_2	0.6
T_3	0.8

Table 3: Parameters of the ellipsoidal flow simulations

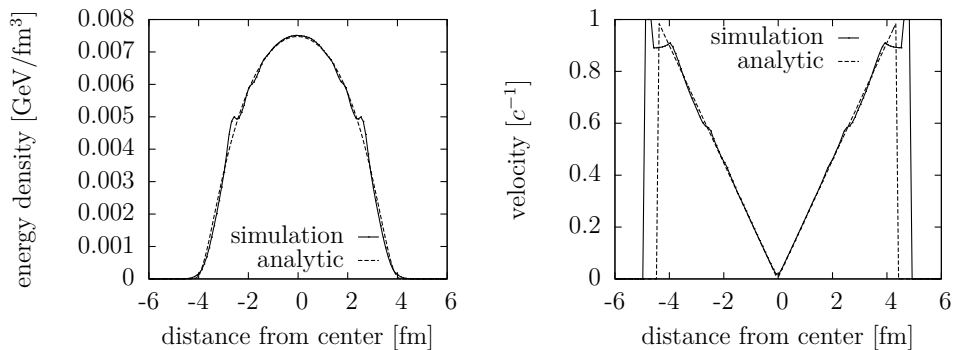


Figure 8: Ellipsoidal flow, energy density in the local rest frame of the fluid (left) and velocity (right), MUSTA-FORCE with Minbee limiter.

shown through the three dimensional solution. This solution, despite being pressureless, most resembles a physically relevant situation. The Minbee limiter has shown again less oscillations than others at the sides.

4 Conclusions

As a result of this paper, we have implemented and tested a MUSTA-FORCE algorithm dedicated to solving conservative field equations. The universal MUSTA-FORCE algorithm proved to be quite efficient and robust. Despite promising initial results, it turned out that the MUSTA-FORCE produced numerical oscillations. Fig. 10 illustrates two dimensional energy density cross section in the xy plane of the MUSTA-FORCE with Albada limiter.

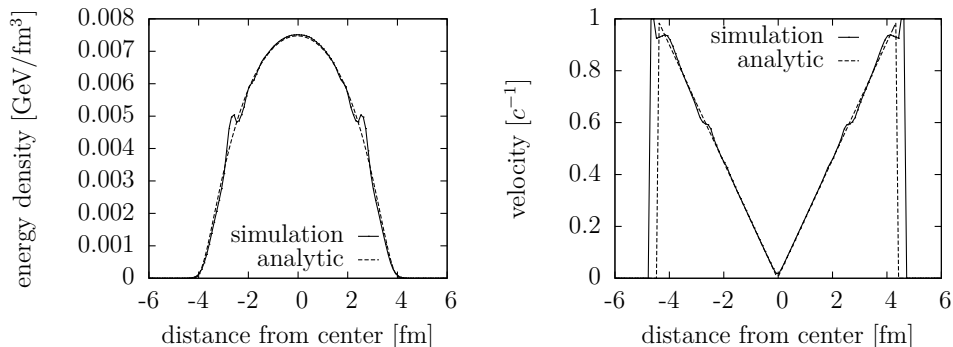


Figure 9: Ellipsoidal flow, energy density in the local rest frame of the fluid (left) and velocity (right), MUSTA-FORCE with van Albada limiter.

It confirms the clearly visible anisotropy of the numerical oscillations. To address this issue, we performed a detailed study of universal slope limiters to reduce oscillations or asymmetric propagation. In all test cases the Minbee limiter has shown the best numerical properties.

This implementation of a relativistic hydrodynamic code is designed to run efficiently on contemporary graphics processing units, which have many times more computing power compared to ordinary CPU processors. Benchmarks and comparison to an equivalent implementation of some of these algorithms in C show speedups of over 2 orders of magnitude. Thanks to such performance levels, event-by-event analyses can be conducted efficiently with a relatively low cost, just a few modern workstations. Our work also provides a framework for implementing other algorithms for high-statistics event-by-event hydrodynamic simulations.

All the calculations were made as fully (3+1)-dimensional simulations in space and in time, without any assumptions regarding its symmetries and without decreasing the dimension of the problem. Such (3+1)-dimensional numerical simulation on high-resolution Cartesian grids is a novel result. It allows us to run hydrodynamic simulations, provide information about properties of the relativistic bulk nuclear matter (QGP) by studying jet-medium interaction and jet-induced flow. Furthermore event-by-event simulations allow us to investigate initial condition fluctuation of the heavy ion collision in the pre-equilibrium stage and it might have an impact on the dynamic in the nuclear medium.

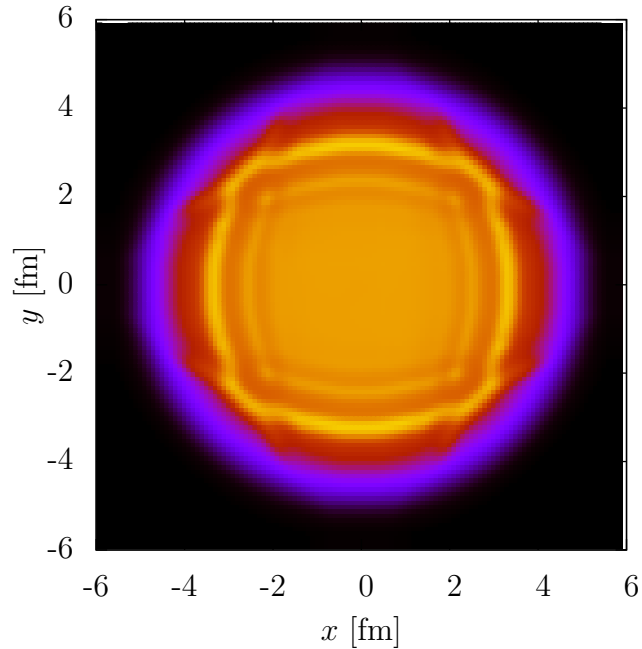


Figure 10: Ellipsoidal flow in the xy plane, energy density in the local rest frame of the fluid, MUSTA-FORCE with van Albada limiter.

References

- [1] E. Gourgoulhon, "An introduction to relativistic hydrodynamics," *EAS Publications Series*, vol. 21, 2008, pp. 43–79.
- [2] P. Huovinen and P. V. Ruuskanen, "Hydrodynamic models for heavy ion collisions," *Ann. Rev. Nucl. Part. Sci.*, vol. 56, 2006, pp. 163–206.
- [3] V. Schneider, U. Katscher, D. H. Rischke, B. Waldhauser, J. A. Maruhn and C.-D. Munz, "New algorithm for ultra-relativistic numerical hydrodynamics," *Journal of Computational Physics*, vol. 105, 1993, pp. 92-107.
- [4] D. S. Balsara, "Riemann solver for relativistic hydrodynamics," *Journal of Computational Physics*, vol. 114, 1994, pp. 284-297.
- [5] H. Cheng, H. Yang, and Y. Zhang, "Riemann problem for the Chaplygin Euler equations of compressible fluid flow." *International Journal of*

- Nonlinear Sciences and Numerical Simulation*, 11 no. 11, 2010, pp. 985-992.
- [6] Y. Akamatsu, S. Inutsuka, C. Nonaka and M. Takamoto, "A new scheme of casual viscous hydrodynamics for relativistic heavy-ion collisions: a Riemann solver for quark-gluon plasma," *Journal of Computational Physics*, vol. 256, 2014, pp. 34-54.
- [7] I. A. Karpenko, P. Huovinen and M. Bleicher, "A 3+1 dimensional viscous hydrodynamic code for relativistic heavy ion collisions," *Computer Physics Communications*, vol. 185, no. 11, pp. 3016-3027, 2014.
- [8] Y. Tachibana and T. Hirano, "Momentum transport away from a jet in an expanding nuclear medium," *Phys. Rev.*, vol. C90, no. 2, pp. 021902, 2014.
- [9] P. Božek, "Flow and interferometry in (3 + 1)-dimensional viscous hydrodynamics," *Phys. Rev. C*, vol. 85, no. 11, pp. 034901–034909, 2012.
- [10] S. V. Akkelin, Y. Hama, Iu. A. Karpenko and Yu. M. Sinyukov, "Hydrokinetic approach to relativistic heavy ion collisions," *Phys. Rev. C*, vol. 78, no. 3, pp. 034906–034920, 2008.
- [11] I. Sagert, W. Bauer, D. Colbry, J. Howell, R. Pickett, A. Staber and T. Strother, "Hydrodynamic shock wave studies within a kinetic Monte Carlo approach," *Journal of Computational Physics*, vol. 266, 2014, pp. 191-213
- [12] J. Gerhard, V. Lindenstruth and M. Bleicher, "Relativistic hydrodynamics on graphic cards," *Comput.Phys.Commun.*, vol. 184, no. 2 2013, pp. 311-319.
- [13] J. P. Boris and D. L. Book, "Flux-corrected transport. I. SHASTA, a fluid transport algorithm that works," *Journal of Computational Physics*, vol. 11, no. 1, pp. 38–69, 1973.
- [14] E. F. Toro, *Multi-stage predictor-corrector fluxes for hyperbolic equations*, Isaac Newton Institute for Mathematical Sciences Preprint Series NI03037-NPA, University of Cambridge, UK, 2003.
- [15] E. F. Toro, "MUSTA: a multi-stage numerical flux," *Appl. Numer. Math.*, vol. 56, no. 10, 2006, pp. 1464–1479.
- [16] S. Cygert, J. Porter-Sobieraj, D. Kikola, J. Sikorski and M. Slodkowski, "Towards an efficient multi-stage Riemann solver for nuclear physics

- simulations," in *Computer Science and Information Systems (FedCSIS), 2013 Federated Conference on*, 2013, pp. 441–446.
- [17] M. L. Miller, K. Reygers, S. J. Sanders and P. Steinberg, "Glauber modeling in high energy nuclear collisions," *Ann.Rev.Nucl.Part.Sci.*, vol. 57, 2007, pp. 205–243.
- [18] K. J. Eskola, H. Niemi and P. V. Ruuskanen, "Elliptic flow from pQCD + saturation + hydro model," *J. Phys. G35*, 2008.
- [19] V. K. Magas, L. P. Csernai and D. Strottman, "Effective string rope model for the initial stages of ultra-relativistic heavy ion collisions," *Nuclear Physics A*, vol. 712, no. 1-2, 2002, pp. 167–204.
- [20] B. Alver, M. Baker, C. Loizides and P. Steinberg, "The PHOBOS Glauber Monte Carlo", 2008, arXiv:0805.4411.
- [21] W. Broniowski, M. Rybczynski and P. Bozek, "GLISSANDO: Glauber initial-state simulation and more," *Comput.Phys.Commun.*, vol. 180, no. 1, 2009, pp. 69–83.
- [22] M. Rybczynski, G. Stefanek, W. Broniowski and P. Bozek, "GLISSANDO 2: Glauber initial-state simulation and more..., ver. 2," *Comput.Phys.Commun.*, vol. 185, no. 6, 2014, pp. 1759-1772.
- [23] H. J. Drescher, S. Ostapchenko, T. Pierog and K. Werner, "Initial condition for QGP evolution from NEXUS," *Phys.Rev. C*, vol. 65:054902, 2002.
- [24] R. Derradi de Souza, J. Takahashi and T. Kodama, "Effects of initial state fluctuations in the final state elliptic flow measurements using the NeXSPheRIO model," *Phys. Rev.*, vol. C85, pp. 054909, 2012.
- [25] T. Pierog, Iu. Karpenko, S. Porteboeuf, S. and K. Werner, "New Developments of EPOS 2," 2010, arXiv:1011.3748.
- [26] S. A. Bass, M. Belkacem, M. Bleicher, M. Brandstetter, L. Bravina et al. "Microscopic models for ultrarelativistic heavy ion collisions," *Prog.Part.Nucl.Phys.*, vol. 41, 1998, pp. 255–369.
- [27] E. F. Toro, *Riemann solvers and numerical methods for fluid dynamics: A practical introduction*, Springer, 1999.
- [28] E.F. Toro, and V.A. Titarev, "MUSTA fluxes for systems of conservation laws" *Journal of Computational Physics*, 216(2), pp.403-429., 2006.

- [29] E. Constantinescu and A. Sandu, "Explicit time stepping methods with high stage order and monotonicity properties," *in Proc. of the 9th International Conference on Computational Science*, 2009, pp. 293–301.
- [30] A. Harten and S. Osher, "Uniformly high-order accurate nonoscillatory schemes," *SIAM Journal on Numerical Analysis*, 1987, pp. 279–309.
- [31] M. Berger, S. M. Murman and M. J. Aftosmis, "Analysis of slope limiters on irregular grids", *In 43rd AIAA Aerospace Sciences Meeting and Exhibit*, 2005.
- [32] P. K. Sweby and M. J. Baines, "Convergence of Roe's scheme for the general non-linear scalar wave equation," *Reading Univ. Numerical Analysis Report*, 1981.
- [33] P. L. Roe, "Some contributions to the modelling of discontinuous flows," *In Proc. AMS/SIAM Seminar*, San Diego, 1983.
- [34] G. D. van Albada, B. van Leer and W. W. Roberts, "A comparative study of computational methods in cosmic gas dynamics," *Astronomy and Astrophysics*, vol. 108, 1982, pp. 76–84.
- [35] B. van Leer, "Towards the ultimate conservative difference scheme, Monotonicity and conservation combined in a second order scheme," *J.Comp.Phys.*, vol. 14, 1974, pp. 361–370.
- [36] D. H. Rischke, "Fluid dynamics for relativistic nuclear collisions," *In Hadrons in Dense Matter and Hadrosynthesis*, Springer Verlag, 1999.
- [37] NVIDIA Corporation: CUDA C Programming Guide, 2014.
- [38] K. W. Thompson, "The special relativistic shock tube," *Journal of Fluid Mechanics*, vol. 171, 1986, pp.365–375.
- [39] J. M. Martí and E. Müller, "Numerical hydrodynamics in special relativity," *Living Rev. Relativity*, vol. 6, 2003.
- [40] M. Chojnacki, W. Florkowski and T. Csörgö, "Formation of Hubble-like flow in little bangs," *Physical Review C*, vol. 71, no. 4, pp. 044902, 2005.
- [41] Yu. M. Sinyukov and Iu. A. Karpenko, "Quasi-inertial ellipsoidal flows in relativistic hydrodynamics," 2005, arXiv:nucl-th/0505041.
- [42] Y. M. Sinyukov and I. A. Karpenko, "Ellipsoidal flows in relativistic hydrodynamics of finite systems" *Acta Physica Hungarica Series A, Heavy Ion Physics*, vol. 25, no. 1, pp. 141–147, 2006.

- [43] P.M. Blakely, N. Nikiforakis, and W.D. Henshaw, "Assessment of the MUSTA approach for numerical relativistic hydrodynamics" *Astronomy and Astrophysics*, 575 (A102), 2015.